Phase-field theory of multicomponent incompressible Cahn-Hilliard liquids

Gyula I. Tóth*
Department of Physics and Technology, University of Bergen, Allégaten 55, N-5007 Bergen, Norway and Wigner Research Centre for Physics, P.O. Box 49, H-1525 Budapest, Hungary

Mojdeh Zarifi and Bjørn Kvamme
Department of Physics and Technology, University of Bergen, Allégaten 55, N-5007 Bergen, Norway
(Received 28 September 2015; revised manuscript received 8 December 2015; published 25 January 2016)

In this paper, a generalization of the Cahn-Hilliard theory of binary liquids is presented for multicomponent incompressible liquid mixtures. First, a thermodynamically consistent convection-diffusion-type dynamics is derived on the basis of the Lagrange multiplier formalism. Next, a generalization of the binary Cahn-Hilliard free-energy functional is presented for an arbitrary number of components, offering the utilization of independent pairwise equilibrium interfacial properties. We show that the equilibrium two-component interfaces minimize the functional, and we demonstrate that the energy penalization for multicomponent states increases strictly monotonously as a function of the number of components being present. We validate the model via equilibrium contact angle calculations in ternary and quaternary (four-component) systems. Simulations addressing liquid-flow-assisted spinodal decomposition in these systems are also presented.

DOI: 10.1103/PhysRevE.93.013126

I. INTRODUCTION

Multicomponent liquid mixtures are of continuously increasing scientific and industrial importance. For instance, it has recently been discovered that controlled pattern formation in ternary colloidal emulsions and polymer mixtures could be used in producing advanced pharmaceutics, biochemical assays, or templating microporous materials [1,2]. Multicomponent emulsions might also play an important role in developing a new, efficient, and environmentally sound enhanced crude oil recovery technique [3–6]. Although numerous theoretical studies addressing binary liquid flows are available, significantly less is known about ternary flows, and much less is known about systems with four or more components. The continuum description of binary systems undergoing phase separation originates from Cahn and Hilliard [7], and it was further improved by Cook [8] and Langer [9,10]. The binary theory was successfully extended also for ternary systems by de Fontaine [11,12], Morral and Cahn [13], Hoyt [14,15], and Maier-Paape *et al.* [16]. Coupling liquid flow to the Cahn-Hilliard theory is also possible on the basis of the Korteweg stress tensor [17,18] (also interpreted as the least action principle in statistical physics [19]), and it has been done for binary systems by several authors [20–22], thus resulting in a reasonable picture of binary liquids [23], while a liquid-flow coupled generalization of the Cahn-Hilliard model for an arbitrary number of components was developed by Kim and Lowengrub [24], and later by Kim [25]. The Kim-Lowengrub model was tested mainly for the ternary case, while quite limited calculations are available for four-component systems. Furthermore, as will be demonstrated in this paper, the construction of neither the free-energy functional nor the diffusion equations used by Kim and Lowengrub satisfies all conditions of physical and mathematical consistency, or if so, the constraints on the model parameters strongly limit the applicability of the theory. Therefore, the problem needs further investigation.

The main difficulty in describing many-component flows is finding appropriate extensions of both the thermodynamic functions and the dynamic properties for high-order multiple junctions. This is far from being trivial, mostly due to the lack of microscopic data. Nevertheless, one can extrapolate from the binary interfaces while maintaining physical and mathematical consistency. In the case of spinodal decomposition, for example, physical consistency means that the multicomponent states of the material should be energetically less and less favorable with an increasing number of components. Consequently, the system should converge to equilibrium configurations showing a single-component—binary interface—trijunction topology. The conditions of mathematical consistency can be summarized as the *condition of formal reducibility*, i.e., writing up the model for N components and then setting the Nth component to zero should result in the $N-1$ component model on the level of *both* the free-energy functional and the dynamic equations.

In this work, we formulate such a consistent generalization of the binary Cahn-Hilliard theory for an arbitrary number of components, for which (i) the bulk states are absolute minima of the free-energy functional, (ii) the two-component equilibrium interfaces represent stable equilibrium, and (iii) the energy of multiple junctions increases as a function of the number of components. In addition, the free-energy density landscape has no multicomponent local minima, therefore the system cannot get trapped into a multicomponent homogeneous state during spinodal decomposition. Furthermore, a convection-diffusion dynamics is also developed, which (i) does not label the variables in principle, and (ii) extends (reduces) naturally, when a component is added to (removed from) the model.

The paper is structured as follows. In Sec. II, we define first the relevant variables describing a multicomponent liquid flow, together with introducing a general free-energy functional formalism. Next, we study equilibrium via the Euler-Lagrange

*Gyula.Toth@ift.uib.no

equations, and we construct a general convection-diffusion dynamics. The application of the general framework for multicomponent spinodal decomposition follows then in Sec. III. We construct a consistent extension of the binary Cahn-Hilliard free-energy functional for an arbitrary number of components, and we demonstrate both the physical and mathematical consistency of our approach. After presenting the numerical methods in Sec. IV, the validation of the model follows in Sec. V, including equilibrium contact angle measurements and modeling spinodal decomposition in both ternary and quaternary systems. The conclusions are summarized in Sec. VI.

II. THEORETICAL FRAMEWORK

A. Energy functional formalism

Consider a system of N incompressible liquids of unique mass density ρ. In a mixture of the liquids, the *mass fraction* of component i reads $c_i = m_i/m$, where m_i is the mass of component i and $m = \sum_{i=1}^{N} m_i$ is the total mass in a control volume V. The mass fractions then sum up to 1 by definition, i.e., $\sum_{i=1}^{N} c_k = 1$. Taking the limit $V \to 0$, all quantities become local, therefore the (local and temporal) *conserved* composition fields $c_i \to c_i(\mathbf{r},t)$ characterizing an inhomogeneous system can be introduced. The relation $\sum_{i=1}^{N} c_i = 1$ transforms then into the following *local* constraint:

$$\sum_{i=1}^{N} c_i(\mathbf{r},t) = 1. \tag{1}$$

We assume that the Helmholtz free energy of the inhomogeneous nonequilibrium system can be expressed as a *functional* of the fields:

$$F = \int dV \{ f[c_i(\mathbf{r},t), \nabla c_i(\mathbf{r},t)] \}, \tag{2}$$

where the integrand is a function of the fields and their gradients. This type of energy functional is called square gradient theory. In the literature, the local constraint is often handled by eliminating one of the components already at the level of the free-energy functional, thus resulting in an unconditional system. In contrast, Eq. (1) is taken into account here by using a Lagrange multiplier as

$$\tilde{F} := F - \int dV \left\{ \Lambda(\mathbf{r},t) \left[\sum_{i=1}^{N} c_i(\mathbf{r},t) - 1 \right] \right\}, \tag{3}$$

where $\tilde{F}$ is the *conditional* free-energy functional and $\Lambda(\mathbf{r},t)$ is the Lagrange multiplier. In our derivations, we will use this general formalism to derive consistent dynamic equations for the system.

B. Equilibrium

Equilibrium solutions represent extrema (minimum, maximum, or saddle) of the free-energy functional, therefore they can be determined by solving the following Euler-Lagrange equations:

$$\frac{\delta \tilde{F}}{\delta c_i} = \frac{\delta F}{\delta c_i} - \lambda(\mathbf{r}) = \tilde{\mu}_i^0, \tag{4}$$

where $\delta F/\delta c_i$ is the functional derivative of F with respect to $c_i(\mathbf{r})$ $(i = 1, \ldots, N)$, whereas $\tilde{\mu}_i^0 = [(\delta F/\delta c_i) - \Lambda(\mathbf{r})]_{\mathbf{c}_0}$ is a diffusion potential belonging to a homogeneous reference state $\mathbf{c}_0 = (c_1^0, c_2^0, \ldots, c_N^0)$. Since the variables are conserved, the Lagrange multiplier cannot be expressed directly from Eq. (4). Nevertheless, one can take the gradient of Eq. (4) to eliminate the constant μ_i' [also containing the background value of $\lambda(\mathbf{r})$], yielding

$$\nabla \frac{\delta F}{\delta c_i} = \nabla \lambda(\mathbf{r}), \tag{5}$$

or, equivalently,

$$\nabla \left(\frac{\delta F}{\delta c_i} - \frac{\delta F}{\delta c_j} \right) = 0 \tag{6}$$

for any (i,j) pairs. In general, $\nabla\lambda(\mathbf{r})$ can be eliminated from Eq. (5) as follows. Multiplying the equations by arbitrary weights $A_i \neq 0$ and then summing them for $i = 1, \ldots, N$ results in

$$\nabla \lambda(\mathbf{r}) = \sum_{i=1}^{N} a_i \nabla \frac{\delta F}{\delta c_i}, \tag{7}$$

where $a_i = A_i / \sum_{k=1}^{N} A_k \neq 0$ is a normalized coefficient, i.e., $\sum_{i=1}^{N} a_i = 1$. Substituting Eq. (7) into Eq. (5) and then rewriting the equations in matrix form results in

$$(\mathbb{I} - \mathbf{e} \otimes \mathbf{a}) \cdot \nabla \frac{\delta F}{\delta \mathbf{c}} = 0, \tag{8}$$

where $\mathbb{I}$ is the $N \times N$ identity matrix, $\mathbf{e} = (1,1,\ldots,1)^T$ is a column, while $\mathbf{a} = (a_1, a_2, \ldots, a_N)$ is a row vector, $\otimes$ denotes the dyadic (tensor or direct) product, and $\delta F/\delta \mathbf{c} = (\delta F/\delta c_1, \delta F/\delta c_2, \ldots, \delta F/\delta c_N)^T$ is the column vector of the functional derivatives. Note that the matrix $\mathbb{A} = \mathbb{I} - \mathbf{e} \otimes \mathbf{a}$ has a *single* eigenvalue $s = 0$ with eigenvector $\mathbf{e}$, thus prescribing equal functional derivative gradients in equilibrium, independent from the weights $\mathbf{a}$. (In other words, $\mathbf{e}$ is the algebraic representation of equilibrium.) Consequently, the solution of Eq. (5) coincides with the solution of Eq. (6) for arbitrary positive $\{A_i\}$ weights.

C. Dynamic equations

1. Diffusion equations

Incompressible multicomponent flow is governed by *convection-diffusion*-type dynamics. We start the derivation of the kinetic equations following Kim and Lowengrub [24]. The diffusion equations follow from the mass balance for the individual components, thus resulting in [24]

$$\rho\, \dot{c}_i = \nabla \cdot \mathbf{J}_i, \tag{9}$$

where $\dot{c}_i = \partial c_i/\partial t + \mathbf{v} \cdot \nabla c_i$ is the material derivative and $\mathbf{v} = \sum_{i=1}^{N} c_i \mathbf{v}_i$ is the mixture velocity, where $\mathbf{v}_i$ is the individual velocity field of the ith component. Furthermore, $\sum_i \mathbf{J}_i = 0$ applies for the diffusion fluxes $\mathbf{J}_i = c_i \rho(\mathbf{v} - \mathbf{v}_i)$, ensuring thus $\sum_{i=1}^{N} \dot{c}_i(\mathbf{r},t) = 0$. The diffusion fluxes can then be constructed as

$$\mathbf{J}_i := \nu_i \nabla \tilde{\mu}_i \tag{10}$$

(for example), where $\nu_i > 0$ is the diffusion mobility of component i, and $\tilde{\mu}_i = \delta\tilde{F}/\delta c_i = \delta F/\delta c_i - \Lambda(\mathbf{r},t)$ is the generalized nonequilibrium chemical potential. Note that in equilibrium $\tilde{\mu}_i \to \tilde{\mu}_i^0$ (constant), thus indicating $\mathbf{J}_i = \mathbf{0}$ and (consequently) $\dot{c}_i = 0$. The Lagrange multiplier can be expressed as $\nabla\Lambda(\mathbf{r},t) = \sum_{i=1}^{N} \tilde{\nu}_i \nabla(\delta F/\delta c_i)$, where $\tilde{\nu}_i = \nu_i / \sum_{j=1}^{N} \nu_j > 0$. Using this in Eq. (9), and introducing $\nu_i := \kappa_i \Sigma$ (where $\Sigma = \sum_{k=1}^{N} \kappa_k$), results in

$$\mathbf{J}_i = \sum_{j=1}^{N} \kappa_{ij} \nabla\left(\frac{\delta F}{\delta c_i} - \frac{\delta F}{\delta c_j}\right), \tag{11}$$

where $\kappa_{ij} = \kappa_i \kappa_j$. Comparing Eqs. (11) and (6), however, indicates $\mathbf{J}_i = \mathbf{0}$ in equilibrium for *arbitrary* κ_{ij}'s. The only condition for the mobilities emerges from the symmetry argument that the variables should not be labeled, where labeling means that the time evolution of the system is not invariant under relabeling the variables. The condition of no labeling yields [26]

$$\kappa_{ij} = \kappa_{ji}, \tag{12}$$

in agreement with Onsager's approach of multicomponent diffusion [27]. In the Appendix of our recent study [26], we pointed out that elimination of one of the variables by setting up $\mathbf{J}_i \propto (\delta F/\delta c_i) - (\delta F/\delta c_N)$ for $i = 1,\ldots,N-1$ labels the variables in principle, and contradicts Onsager's reciprocal relations. Note that Eqs. (11) and (12) offer a more general form for the constitutive equation than Eq. (10). In the latter, we have only N independent parameters, $\vec{\kappa} = (\kappa_1,\kappa_2,\ldots,\kappa_N)$, and the mobility matrix $\mathbb{L}$ in the general form $\rho\,\dot{\mathbf{c}} = \nabla\cdot(\mathbb{L}\cdot\nabla\vec{\mu})$ emerges from these as $\mathbb{L} = \vec{\kappa}\otimes\vec{\kappa}$, where $\otimes$ denotes the tensor product. In contrast, according to Eqs. (11) and (12), we may choose $N(N-1)/2$ free parameters $\{\kappa_{ij}\}$ in general, and the elements of the mobility matrix are calculated as $L_{ii} = \sum_{j\neq i} \kappa_{ij}$ and $L_{ij} = -\kappa_{ij}$ for $i \neq j$. Although Eqs. (10) and (11) coincide in equilibrium, the general construction becomes significant for $N \geqslant 4$, where the number of pairs is greater than N.

The remaining issue that has to be considered is the condition of "formal reducibility" for the dynamic equations. An elegant solution of the problem introducing mobility matrices on a geometric basis was published by Bollada, Jimack, and Mullis [28]. They proposed symmetric mobility matrices reducing formally. For example, in the case of $\kappa_{ij}(c_i,c_j) = [c_i/(1-c_i)][c_j/(1-c_j)]$, the kth row and column of the mobility matrix vanish, and the mobility matrix of an $(N-1)$-component system is recovered. Note, however, that such a mobility matrix can be "dangerous" with respect to the free-energy functional, meaning that nonequilibrium states may become stationary since the Eq. (6) is not a necessary condition for a stationary solution. Speaking mathematically more precisely, the eigenvalue $s = 0$ (representing the stationary solution) of the mobility matrix $\mathbb{L}$ has multiplicity greater than 1 in the case of at least one vanishing field. The components of the corresponding eigenvectors are equal at the positions of nonvanishing fields, otherwise they are arbitrary. *Therefore, a stationary state of the dynamics does not necessarily represent an equilibrium solution*. Nevertheless, as discussed in our recent paper [26], if one can prove that the $(n+m)$-component natural extensions of all equilibrium solutions emerging from the n-component model also represent equilibrium in the $(n+m)$-component model for any $n,m \geqslant 1$, then the Bollada-Jimack-Mullis matrix is not dangerous with respect to the free-energy functional. Having such a functional, although necessary, is not satisfactory since the dynamics must satisfy also the *second law of thermodynamics*, i.e., the entropy production rate must be non-negative. This requirement can be addressed by considering the Kim-Lowengrub model in the constant density limit. The condition for the contribution of the diffusion equations to the entropy production rate reads [24]

$$\sum_{i=1}^{N} \nabla\hat{\mu}_i \cdot \mathbf{J}_i \geqslant 0. \tag{13}$$

Here $\hat{\mu}_i = (\delta F/\delta c_i) + p$, where p is the nonequilibrium thermodynamic pressure. According to Eq. (11), $\mathbf{J}_i = \sum_{j=1}^{N} L_{ij}\nabla(\delta F/\delta c_j)$, where $\sum_{j=1}^{N} L_{ij} = 0$, therefore Eq. (13) results in

$$\sum_{i,j} L_{ij}\left(\nabla\frac{\delta F}{\delta c_i}\cdot\nabla\frac{\delta F}{\delta c_j}\right) \geqslant 0, \tag{14}$$

thus indicating that the mobility matrix $\mathbb{L}$ must be *positive-semidefinite*. Therefore, the original Bollada-Jimack-Mullis matrix is modified as

$$\kappa_{ij}(c_i,c_j) := \kappa_{ij}^0 \left|\frac{c_i}{1-c_i}\right|\left|\frac{c_j}{1-c_j}\right|, \tag{15}$$

where $\kappa_{ij}^0 > 0$'s are arbitrary constants. The absolute value is necessary for a simple reason: The solution may slightly leave the physical regime ($0 \leqslant c_i \leqslant 1$ for $i = 1,\ldots,N$) in the simulations because of numerical reasons. Nevertheless, small perturbations around *stable* equilibrium solutions relax naturally for a positive-semidefinite mobility matrix without any further artificial modifications, such as overwriting the solution. This should be true for at least the bulk components and the binary equilibrium interfaces. The positive semidefiniteness of this matrix has been verified numerically case by case for the particular matrices we used in our calculations and simulations.

2. *Navier-Stokes equation*

The velocity field is governed by the following Navier-Stokes equation (emerging from the momentum balance for the components) [24]:

$$\rho\,\dot{\mathbf{v}} = \nabla\cdot(\mathbb{R}+\mathbb{D}), \tag{16}$$

where $\mathbb{R}$ and $\mathbb{D}$ are the reversible and irreversible stresses, respectively. The viscous stress of a multicomponent Newtonian liquid can be approximated as

$$\mathbb{D} = \eta[(\nabla\otimes\mathbf{v}) + (\nabla\otimes\mathbf{v})^T], \tag{17}$$

where $\eta = \sum_{i=1}^{N} c_i\eta_i$ is the local shear viscosity, calculated from the viscosities of the bulk components, η_i. Furthermore, the reversible stress has the general Korteweg form [17,18]

$$\mathbb{R} = -\tilde{p}\,\mathbb{I} + \mathbb{A}, \tag{18}$$

where $\tilde{p}$ is a nonequilibrium generalization of the equilibrium thermodynamic pressure:

$$-\tilde{p} = \tilde{f} - \sum_{i=1}^{N} c_i \frac{\delta \tilde{F}}{\delta c_i} = -p + \Lambda(\mathbf{r},t), \tag{19}$$

where $\tilde{f}$ is the integrand of $\tilde{F}$ defined by Eq. (3), and $-p = f - \sum_{x=1}^{N} c_i(\delta F/\delta c_i)$. Furthermore, $\mathbb{A}$ is a general nondiagonal tensor, which can be determined from the condition of mechanical equilibrium, often formulated as a generalized Gibbs-Duhem relation [19–21]

$$\nabla \cdot \mathbb{R} = -\sum_{i=1}^{N} c_i \nabla \frac{\delta \tilde{F}}{\delta c_i}. \tag{20}$$

Using Eq. (18) in (20) then yields

$$\mathbb{A} = -\sum_{i=1}^{N} \left(\nabla c_i \otimes \frac{\partial f}{\partial \nabla c_i} \right), \tag{21}$$

showing that the flow operator does not contain the Lagrange multiplier. This result is in agreement with previous results [24]. Furthermore, since the liquid mixture is incompressible and all the components have the same density, we also have the condition

$$\nabla \cdot \mathbf{v} = 0. \tag{22}$$

Although this condition results in a *degeneracy* in the velocity field, it is resolved by the Lagrange multiplier $\Lambda(\mathbf{r},t)$ in Eq. (19).

III. MULTICOMPONENT CAHN-HILLIARD LIQUID

A. Free-energy functional

The free-energy functional of a general, multicomponent Cahn-Hilliard liquid is formulated as [26]

$$F = \int dV \left\{ f(\mathbf{c}) + \frac{\epsilon^2(\mathbf{c})}{2} \sum_{i=1}^{N} (\nabla c_i)^2 \right\}, \tag{23}$$

where the *multiwell* free-energy landscape $f(\mathbf{c})$ is constructed as [26]

$$f(\mathbf{c}) := w(\mathbf{c})\, g(\mathbf{c}) + A_3 f_3(\mathbf{c}), \tag{24}$$

where

$$g(\mathbf{c}) = \frac{1}{12} + \sum_{i=1}^{N} \left(\frac{c_i^4}{4} - \frac{c_i^3}{3} \right) + \frac{1}{2} \sum_{i<j} c_i^2 c_j^2. \tag{25}$$

In Eq. (25), the double sum stands for a summation for all pairs, i.e., $\sum_{i<j} = \sum_{i=1}^{N-1} \sum_{j=i+1}^{N}$. Following Kazaryan [29], the coefficients $w(\mathbf{c})$ and $\epsilon^2(\mathbf{c})$ interpolating between the component pairs read

$$w(\mathbf{c}) = \frac{\sum_{i<j} w_{ij} c_i^2 c_j^2}{\sum_{i<j} c_i^2 c_j^2} \quad \text{and} \quad \epsilon^2(\mathbf{c}) = \frac{\sum_{i<j} \epsilon_{ij}^2 c_i^2 c_j^2}{\sum_{i<j} c_i^2 c_j^2}. \tag{26}$$

Furthermore, the "triplet" term is defined as

$$f_3(\mathbf{c}) := \sum_{i<j<k} |c_i|\,|c_j|\,|c_k|, \tag{27}$$

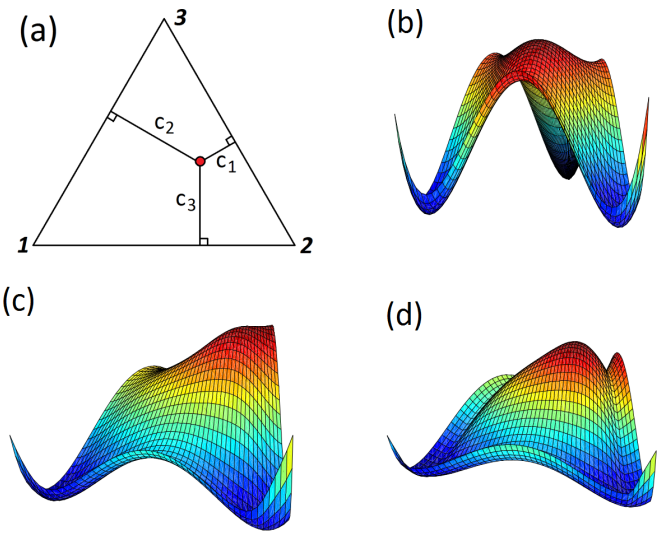

FIG. 1. Gibbs simplex and free-energy landscapes $f(\mathbf{c})$ in ternary systems. (a) Gibbs simplex in a ternary system. The compositions in the red dot are measured perpendicular to the edges of the triangle. If all the edges measure 1 unit, $c_1 + c_2 + c_3 = 1$. The vertices (denoted by bold numbers) correspond to bulk components, i.e., $c_i = 1$ at vertex i, where $i = 1,2,3$. (b) Free-energy density in the symmetric system without a triplet term (i.e., $A_3 = 0$). (c) and (d) Free-energy landscapes in an asymmetric ternary system ($w_{12} = 1.5\, w_0$, $w_{13} = 1.0\, w_0$, and $w_{23} = 0.5\, w_0$) in the case of $A_3 = 0$ (c) and $A_3 = 1.0\, w_0$ (d). The minima of the free-energy landscapes correspond to the vertices of the Gibbs simplex displayed in panel (a).

where the sum is for all different (i,j,k) triplets, i.e., $i \neq j, i \neq k$, and $j \neq k$, $i,j,k = 1,\ldots,N$. The usual (Gibbs-simplex) representation of the free-energy landscape is shown in Figs. 1(a)–1(d) for symmetric and asymmetric ternary systems in the case of $A_3 = 0$ and $A_3 \neq 0$, respectively. We note that similar terms are used by some authors [30,31] to control the presence of the third component at binary interfaces, however our approach is quite different from theirs, as will be shown.

B. Interfaces, energy hierarchy, and stability

When exactly two components are present, i.e., $c_i + c_j = 1$ for $i \neq j$ and $c_k = 0$ for all $k \neq i,j$, Eq. (23) reduces to the usual binary Cahn-Hilliard free-energy functional:

$$F_{ij} = \int dV \left\{ w_{ij}[c(1-c)]^2 + \epsilon_{ij}^2 (\nabla c)^2 \right\}, \tag{28}$$

therefore ϵ_{ij}^2's and w_{ij}'s can be related to the interfacial tension (σ_{ij}) and interface thickness (δ_{ij}) as

$$w_{ij} = 3(\sigma_{ij}/\delta_{ij}) \quad \text{and} \quad \epsilon_{ij}^2 = 3(\sigma_{ij}\delta_{ij}), \tag{29}$$

where the interface thickness is defined by the binary equilibrium interface solution

$$c_{ij}(x) = \{1 + \tanh[x/(2\,\delta_{ij})]\}/2, \tag{30}$$

while the interfacial tension reads

$$\sigma_{ij} = \int_{-\infty}^{+\infty} dx \{ w_{ij}[c_{ij}(x)]^2 [1 - c_{ij}(x)]^2 + \epsilon_{ij}^2 [\partial_x c_{ij}(x)]^2 \}. \tag{31}$$

The general functional defined by Eq. (23) has two practical features:

(i) F, *together with* $\delta F/\delta c_i$, reduces formally, i.e., writing up F (and $\delta F/\delta c_i$) for N fields and then applying $c_N \equiv 0$ results in the expressions derived directly in the $(N-1)$-component model. This, together with Eq. (15), results in the formal reducibility of the dynamic equations, too.

(ii) All two-component equilibrium interfaces $c_{kl}(x) = \{1+\tanh[x/(2\delta_{kl})]\}/2$ represent equilibrium in the *complete*, N-component model. In other words, *the binary planar interfaces represent equilibrium in the N-component system* (see Appendix A for details).

We mention that the latter does not apply for almost any of the previous multiphase and multicomponent descriptions [26]. Nevertheless, it is an essential feature because of the following: Eq. (30) represents only a *conditional* extremum, since it is calculated in the $c_i + c_j = 1$ binary subspace. Therefore, there is no guarantee that it is also a solution of the complete variational problem defined by Eq. (6). In the case of several existing multiphase descriptions, the situation is indeed as follows: the equilibrium two-component interfaces do not represent equilibrium of the general, N-component model, due to the inconsistent generalization of the free-energy functional. The problem is resolved in various ways, including the introduction of a nonvariational dynamics, degenerate mobility matrix, or penalizing free-energy terms for ternary states, as also discussed in detail in our recent work [26]. In contrast, our description is free of these artificial modifications.

In a symmetric system ($\epsilon_{ij}^2 \equiv \epsilon_0^2$ and $w_{ij} \equiv w_0$) without a triplet energy contribution ($A_3 = 0$), Eq. (24) is a finite-degree polynomial penalizing the multicomponent states as follows:

$$f(\mathbf{c}_n) = \frac{1}{12}\left(1 - \frac{1}{n^2}\right), \tag{32}$$

where $\mathbf{c}_n = \mathcal{P}[\{1/n, 1/n, \ldots, 1/n, 0, 0, \ldots, 0\}]$. Here, $\mathcal{P}[\cdot]$ stands for an arbitrary permutation of the components of the vector argument $\{c_1, c_2, \ldots, c_N\}$, where n elements have the value $1/n$ and all the others are 0, while $n = 1, \ldots, N$. Equation (24) then penalizes equally the n-component states, and the energy increases strictly monotonously as a function of the number of components being present. This feature also applies for *arbitrary* $A_3 \geqslant 0$ in the symmetric system for the triplet term defined by Eq. (27) (see Appendix B for the derivation).

Interestingly, the strictly monotonous tendency of the subspace extrema seems to be valid even for asymmetric systems, however both $f(\mathbf{c}_n)$ and $\mathbf{c}_n$ now have degeneracy, since both the location and the value of the subspace maxima can be different. This is illustrated in Fig. 2, which shows the degenerate hierarchy of the subspace extrema in the case of asymmetry for $N = 4$. Since the $n = 2$- and 3-component subspace maxima of the Gibbs simplex can now be different, one can define a "path" on the Gibbs simplex as follows: A path starts in a vertex (representing a bulk component) and then jumps to the location of the maximum of one of the connecting edges [denoted by $n = 1$ and 2 in Fig. 2(a)]. From here, we jump to the location of the maximum of one of the connecting planes ($n = 3$), while the final point is the location of the global maximum inside the tetrahedron.

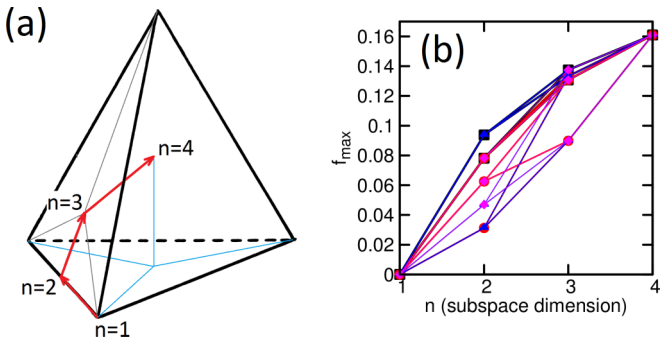

FIG. 2. Degeneracy of the subspace extrema in an asymmetric quaternary system ($w_{12} = 1.25\,w_0$, $w_{13} = 1.5\,w_0$, $w_{23} = 0.5\,w_0$, $w_{14} = 1.25\,w_0$, $w_{24} = 1.0\,w_0$, and $w_{34} = 0.75\,w_0$), for $A_3 = 1.0\,w_0$. (a) A possible path starts in a vertex ($n = 1$) representing the absolute minimum of the free-energy density, then passes the location of a binary ($n = 2$) and a ternary ($n = 3$) maximum, and finally arrives at the location of the single quaternary ($n = 4$) maximum, which is the absolute maximum of the free-energy density. (b) Sequences of subspace extrema along all possible paths illustrated in panel (a).

Figure 2(b) shows the energy density in the subspace maxima (symbols) along all possible bulk → binary → ternary → quaternary paths (denoted by the connecting lines). It seems that all the 24 possible paths prescribe a strictly monotonously increasing energy sequence. If the free-energy landscape does not have any other extrema, and all the extrema except the vertices represent maxima, then this behavior, together with the fact that the free-energy functional penalizes any spatial variation of the fields, suggests that an N-component system undergoes spinodal decomposition, and without becoming trapped into a high-order state, i.e., the system never prefers high-order multiple junctions, independent from the number of components.

Although we constructed a free-energy functional, which is expected to result in spinodal decomposition for an energy-minimizing dynamics, and for which the binary planar interfaces together with the bulk states are equilibrium solutions, the interfaces may become unstable in the case of asymmetry for $A_3 = 0$. The reason is that the $A_3 = 0$ free-energy landscape is "weak" for the multicomponent states, meaning that the energy increases too slowly as a function of n: the energy difference between $f(1,0,\ldots)$ and $f(1/2,1/2,0,\ldots)$ is much more significant than that between $f(1/2,1/2,0,\ldots)$ and $f(1/3,1/3,1/3,0,\ldots)$ [and so on; see Fig. 1(b) and Eq. (32)]. This means that in the case of asymmetry [see Fig. 1(c)], the shift in the location of the three-component maximum can be significant, and therefore it can destabilize the binary planar interface on the closest edge (or, as a matter of fact, on any other edges, except the one with the lowest interfacial tension). To stabilize the (otherwise equilibrium) binary planar interfaces, we apply the triplet term described by Eq. (27). Choosing a sufficiently large amplitude A_3 shifts the location and increases the value of the ternary maximum of the free-energy landscape [see Fig. 1(d)], thus resulting in the restabilization of the interfaces. The phenomenon is also illustrated in Fig. 3. The figure shows the numerical solution of the one-dimensional Euler-Lagrange problem in

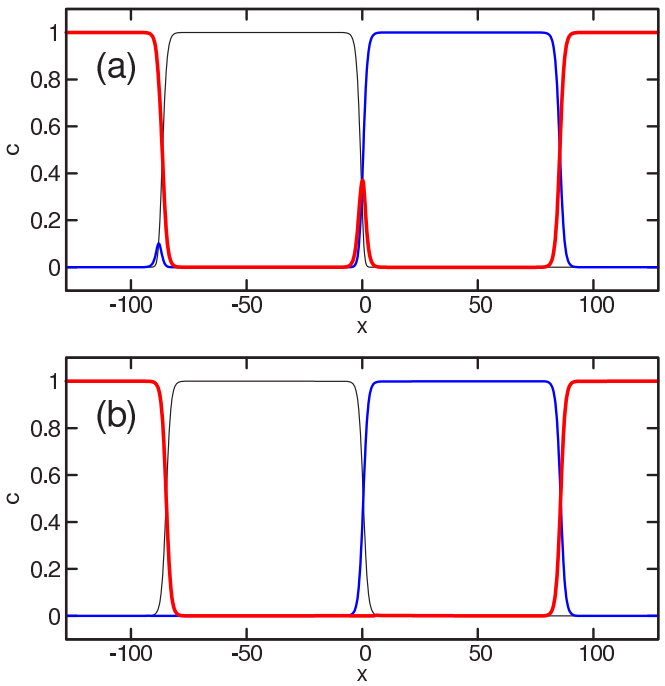

FIG. 3. Two-component equilibrium interfaces in an asymmetric ternary system ($w_{12} = 1.5\,w_0$, $w_{13} = 1.0\,w_0$, and $w_{23} = 0.5\,w_0$) in the case of (a) $A_3 = 0$ and (b) $A_3 = 1.0\,w_0$. Note that in the case of $A_3 = 0$, c_3 (thick red) and c_2 (normal blue) appear on the (1,2) and (1,3) interfaces, respectively, while c_1 (thin black) does not appear on the (2,3) interface, which has the lowest energy. Applying the triplet term then prevents the appearance of the third component at any two-component interfaces.

an asymmetric ternary system for $A_3 = 0$ [panel (a)] and $A_3 \neq 0$ [panel (b)]. We used the finite-difference method with explicit time stepping to solve the Euler-Lagrange problem $\nabla(\delta F/\delta c_i) = \nabla(\delta F/\delta c_j)$, together with periodic boundary conditions. As one can see, the third component appears at both the (1,2) and (1,3) interfaces in the case of $A_3 = 0$ [see panel (a)], showing that the free-energy landscape is weak with respect to the gradient term, and the binary planar interfaces, although representing equilibrium, are not stable. The only stable interface is the (2,3) interface, which has the lowest energy. Nevertheless, choosing $A_3 = 1$ solves the problem [see panel (b)], since as the three-component maximum of the free-energy landscape increases, the interfaces become stable.

Summarizing, Eq. (23) prescribes a multicomponent free-energy functional, which results in stable bulk states and binary interfaces in equilibrium even for asymmetric systems, while high-order multiple states are penalized increasingly as a function of the number of the components. This behavior results in spinodal decomposition in a system of an arbitrary number of components. Therefore, Eq. (23) is a suitable generalization of the binary Cahn-Hilliard free-energy functional. The triplet term $f_3(\mathbf{c})$ has no effect on the bulk ($n = 1$) and binary states ($n = 2$), and on the structure and hierarchy of the subspace extrema of the free-energy landscape, but it controls the energy of multicomponent (ternary and up) states. Therefore, it is an ideal tool to control the *stability* of the binary planar interfaces.

C. Parameters and scaling

To anchor the mobilities κ_{ij}^0 in Eq. (15) to measurable quantities, we first take Eq. (9) in the binary limit $c_i = u$, $c_j = 1 - u$, and $c_k = 0$ for $i \neq j$ and $k \neq i, j$. In the case of $\mathbf{v} = \mathbf{0}$, it yields

$$\rho \frac{\partial u}{\partial t} = \kappa_{ij}^0 \nabla \frac{\delta F}{\delta u} \tag{33}$$

and $\partial c_k/\partial t = 0$ for $k \neq i, j$. The functional derivative reads $\delta F/\delta u = 2\{w_{ij}[u(1-u)(1-2u)] - \epsilon_{ij}^2 \nabla^2 u\}$. For $u = \delta u \to 0$, Eq. (33) becomes $\rho(\partial_t \delta u) = 2\kappa_{ij}^0 w_{ij}(\nabla^2 \delta u)$, yielding thus the diffusion constant $D_{ij} = (2\kappa_{ij}^0 w_{ij})/\rho$ of the ith component in the bulk jth component. The mobility is then related to the diffusion constant via

$$\frac{2w_{ij}\kappa_{ij}^0}{D_{ij}} = \frac{2w_{ij}\kappa_{ij}^0}{D_{ji}} = \rho, \tag{34}$$

where the second equation emerges from the symmetry of κ_{ij}^0. Therefore, the diffusion constant of the jth component in the ith one is the same as that of the ith component in the jth one in our approach. Scaling the length as $\mathbf{r} := \lambda \hat{\mathbf{r}}$, and introducing $D_{ij} := D_0 \hat{D}_{ij}$, yields the time scale $\tau = \lambda^2/D_0$ in $t := \tau \hat{t}$, while using $w_{ij} := w_0 \hat{w}_{ij}$ and $\epsilon_{ij}^2 := \epsilon_0^2 \hat{\epsilon}_{ij}^2$ results in the dimensionless diffusion equations

$$\frac{dc_i}{d\hat{t}} = \hat{\nabla} \cdot \hat{\mathbf{J}}_i. \tag{35}$$

The dimensionless diffusion fluxes read

$$\hat{\mathbf{J}}_i = \sum_{j=1}^{N} \hat{\kappa}_{ij}^0 \, h(c_i, c_j) \, \hat{\nabla} \left(\frac{\delta \hat{F}}{\delta c_i} - \frac{\delta \hat{F}}{\delta c_j} \right), \tag{36}$$

$$\frac{\delta \hat{F}}{\delta c_i} = \frac{\partial(\hat{w}\, g + \hat{A}_3\, f_3)}{\partial c_i} + \frac{\delta_0^2}{\lambda^2} \left[\frac{\partial \hat{\epsilon}^2}{\partial c_i} (\hat{\nabla}\mathbf{c})^2 - \hat{\epsilon}^2 \hat{\nabla}^2 c_i \right], \tag{37}$$

where $\delta_0^2 = \epsilon_0^2/w_0$. Furthermore, $h(c_i, c_j) = |c_i/(1-c_i)||c_j/(1-c_j)|$ and

$$2\,\hat{\kappa}_{ij}^0 = \hat{D}_{ij}/\hat{w}_{ij}. \tag{38}$$

The dimensionless coefficients read

$$\hat{w} = \frac{\sum_{i<j} \hat{w}_{ij} c_i^2 c_j^2}{\sum_{i<j} c_i^2 c_j^2} \quad \text{and} \quad \hat{\epsilon}^2 = \frac{\sum_{i<j} \hat{\epsilon}_{ij}^2 c_i^2 c_j^2}{\sum_{i<j} c_i^2 c_j^2}, \tag{39}$$

while $\hat{A}_3 = A_3/w_0$. Introducing the dimensionless interfacial tensions $\sigma_{ij} := \sigma_0 \hat{\sigma}_{ij}$ and interface thicknesses $\delta_{ij} := \delta_0 \hat{\delta}_{ij}$, and considering $\epsilon_{ij}^2 = 3(\sigma_{ij}\delta_{ij})$ and $w_{ij} = 3(\sigma_{ij}/\delta_{ij})$, yield the scales

$$\epsilon_0^2 = 3(\sigma_0 \delta_0) \quad \text{and} \quad w_0 = 3(\sigma_0/\delta_0) \tag{40}$$

and

$$\hat{\epsilon}_{ij}^2 = \hat{\sigma}_{ij}\hat{\delta}_{ij} \quad \text{and} \quad \hat{w}_{ij} = \hat{\sigma}_{ij}/\hat{\delta}_{ij}. \tag{41}$$

Furthermore, $\epsilon_0^2/w_0 = \delta_0^2$ in Eq. (37). The dimensionless Navier-Stokes equation reads

$$\frac{d\hat{\mathbf{v}}}{d\hat{t}} = \hat{\boldsymbol{\nabla}} \cdot \hat{\mathbb{P}}, \tag{42}$$

where

$$\hat{\mathbb{P}} = \hat{a}\,\hat{\mathbb{A}}(\mathbf{c}) + \hat{\eta}\,\hat{\mathbb{D}}(\hat{\mathbf{v}}). \tag{43}$$

Here the dimensionless flow-field generator $\hat{\mathbb{A}}(\mathbf{c})$ and the viscous stress $\hat{\mathbb{D}}(\hat{\mathbf{v}})$ read

$$\hat{\mathbb{A}}(\mathbf{c}) = -\hat{\epsilon}^2 \sum_{i=1}^{N} (\hat{\boldsymbol{\nabla}} c_i \otimes \hat{\boldsymbol{\nabla}} c_i), \tag{44}$$

$$\hat{\mathbb{D}}(\hat{\mathbf{v}}) = (\hat{\boldsymbol{\nabla}} \otimes \hat{\mathbf{v}}) + (\hat{\boldsymbol{\nabla}} \otimes \hat{\mathbf{v}})^T, \tag{45}$$

respectively, whereas the dimensionless amplitudes are

$$\hat{a} = \frac{3\sigma_0\delta_0}{D_0^2\rho} \quad \text{and} \quad \hat{\eta} = \frac{\eta}{D_0\rho}. \tag{46}$$

Finally, the incompressibility condition simply becomes

$$\hat{\boldsymbol{\nabla}} \cdot \hat{\mathbf{v}} = \mathbf{0}. \tag{47}$$

IV. NUMERICAL METHOD

The system of dynamic equations described by (35), (42), and (47) is solved numerically on a fully periodic two-dimensional domain by using an operator-splitting-based quasispectral semi-implicit time-stepping scheme [32] combined with the spectral Chorin's projection method as follows. The dynamic equations can be rewritten in the form

$$\frac{\partial \mathbf{y}}{\partial t} = \mathbf{f}(\mathbf{y}, \boldsymbol{\nabla} \cdot \mathbf{y}), \tag{48}$$

where $\mathbf{y} = (c_1, c_2, \ldots, c_n, v_x, v_y)$, and $\mathbf{f}(\mathbf{y}, \boldsymbol{\nabla} \cdot \mathbf{y})$ is the (generally nonlinear) right-hand side. $f(\mathbf{y}, \boldsymbol{\nabla} \cdot \mathbf{y})$ is calculated at time point t, while $\partial y_i/\partial t$ is discretized simply as

$$\frac{\partial y_i}{\partial t} \approx \frac{y_i^{t+\Delta t} - y_i^t}{\Delta t}. \tag{49}$$

Next, we add the general linear term $\hat{s}[y_i] = \sum_{i=1}^{\infty}(-1)^i s_i \nabla^{2i} y_i$ (where $s_i \geqslant 0$) to both sides of Eq. (48). We consider this term at $t + \Delta t$ on the left-hand side, but at t on the right-hand side of the equation. This concept, together with Eq. (49), results in the following, explicit spectral time-stepping scheme:

$$y_i^{t+\Delta t}(\mathbf{k}) = y_i^t(\mathbf{k}) + \frac{\Delta t}{1 + s_i(\mathbf{k})\Delta t} \mathcal{F}\{f_i[\mathbf{y}^t(\mathbf{r}), \boldsymbol{\nabla} \cdot \mathbf{y}^t(\mathbf{r})]\}, \tag{50}$$

where $s_i(\mathbf{k}) = \sum_{j=1}^{\infty} s_j^{(i)} (\mathbf{k}^2)^j$, and $\mathcal{F}\{\cdot\}$ stands for the Fourier transform. The *splitting constants* $\{s_j^{(i)}\}$ must be chosen so that Eq. (50) is stable. Suitable splitting constants can be found by expanding the right-hand side of the differential equations, then identifying terms of the form $(-1)^{n+1} f(\mathbf{y}) \nabla^{2n} y_i$ ($n = 1, 2, \ldots$) in the equation for y_i. $\max\{0, \max\{f(\mathbf{y})\}\}$ then provides a theoretical splitting constant $\tilde{s}_n^{(i)}$. Since the equations are coupled and highly nonlinear, a unique experimental multiplier s is applied, i.e., the splitting constants are chosen as $s_n^{(i)} := s\,\tilde{s}_n^{(i)}$. In our case, we used $s = 5$.

Considering the Navier-Stokes equation, note that the new velocity field $\mathbf{v}^{t+\Delta t}(\mathbf{r})$ does not satisfy Eq. (47) in general. Introducing $\mathbf{v}^{t+\Delta t} := \mathbf{v}^* + \delta\mathbf{v}$, where $\mathbf{v}^*$ is calculated from Eq. (50), and the correction is given in the form $\delta\mathbf{v} := \boldsymbol{\nabla} s(\mathbf{r})$, where $s(\mathbf{r})$ is a scalar field, and using Eq. (47) yields the spectral solution

$$\delta\mathbf{v}(\mathbf{k}) = -\frac{\mathbf{k} \otimes \mathbf{k}}{\mathbf{k}^2} \mathbf{v}^*(\mathbf{k}). \tag{51}$$

Using Eqs. (50) and (51), the velocity field is then generated by the following sequence:

$$\mathbf{v}^*(\mathbf{k}) = \mathbf{v}^t(\mathbf{k}) + \frac{\Delta t}{1 + s_v(\mathbf{k})\Delta t} \mathcal{F}\{\mathbf{f}^t(\mathbf{r})\}, \tag{52}$$

$$\mathbf{v}^{t+\Delta t}(\mathbf{k}) = [\mathbb{I} - \mathbb{P}(\mathbf{k})] \cdot \mathbf{v}^*(\mathbf{k}), \tag{53}$$

where $s_v(\mathbf{k})$ is a splitting function emerging from the viscous stress, $\mathbf{f}^t(\mathbf{r}) = \boldsymbol{\nabla} \cdot \hat{\mathbb{P}}$, where $\hat{\mathbb{P}}$ is defined by Eq. (43), while $\mathbb{P}(\mathbf{k}) = (\mathbf{k} \otimes \mathbf{k})/\mathbf{k}^2$ is the operator generating the divergent part of a vector field. Indeed, in Eq. (53) $\mathbb{I} - \mathbb{P}(\mathbf{k})$ eliminates the divergence of $\mathbf{v}^*$.

It is important to note that our numerical scheme is *unbounded*, meaning that the spatial solution $c_i(\mathbf{r},t)$ might become negative or greater than 1 because of numerical errors. Nevertheless, the construction of the free-energy functional and the modified Bollada-Jimack-Mullis mobility matrix ensures that no artificial modification of the solution is needed after a time step, as discussed before. Instead, the system naturally finds the bulk states and the two-component interfaces. Finally, we mention that the generalized Chorin's projection method presented here is compatible with equilibrium. In equilibrium, the diffusion fluxes vanish, i.e., $\mathbf{J}_i = \mathbf{0}$ for $i = 1, \ldots, N$, resulting in $\dot{\mathbf{c}} = \mathbf{0}$. Furthermore, $\boldsymbol{\nabla} \cdot \mathbb{A}$ becomes the gradient of a scalar function in equilibrium, which is then eliminated by Chorin's projection method (i.e., no flow is generated). Since the viscous terms vanish for a homogeneous velocity field, $\mathbf{v}(\mathbf{r}) = \text{const}$ is the general equilibrium solution.

V. RESULTS

The numerical simulations were performed on a two-dimensional, uniform rectangular grid with spatial resolution $h = 0.5$ and different time steps. The physical parameters were chosen to model realistic binary, ternary, and quaternary (four-component) systems mimicking the oil-water-CO_2 interfaces. The scales then read $\rho = 1000\ \text{kg/m}^3$, $D_0 = 5 \times 10^{-10}\ \text{m}^2/\text{s}$, $\sigma_0 = 50\ \text{mJ/m}^2$, $\delta_0 = 1.25$ Å, and

$$\eta(\mathbf{c}) := \eta_0 \sum_{i=1}^{N} c_i x_i, \tag{54}$$

where $x_i = \eta_i/\eta_0$, and the viscosity scale reads $\eta_0 = 1$ mPa s.

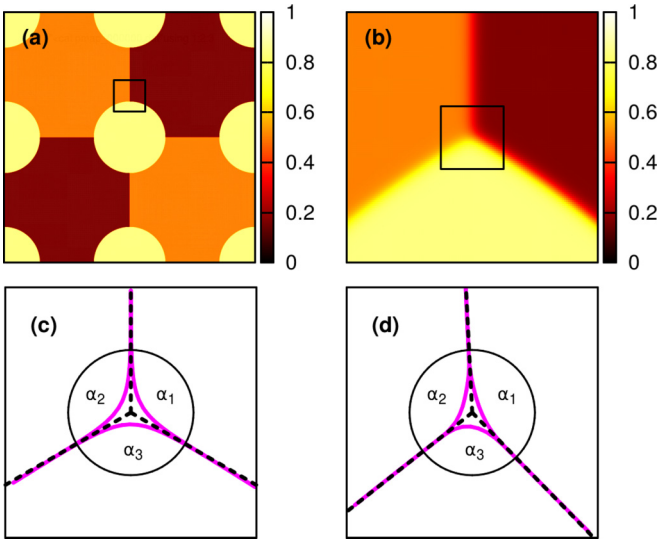

FIG. 4. Contact angle measurement in a ternary system: (a) Initial condition, and (b) converged (equilibrium) solution in a symmetric system in the area indicated by the black square in panel (a). In both panels, $\sum_{i=1}^{3} c_i(\mathbf{r})[(i-0.5)/3]$ is shown. (c) Contour lines $[c_i(\mathbf{r}) = 0.5$ for $i = 1,\ldots,3]$ of the fields at a trijunction in the area indicated by the black square in panel (b), and (d) the same as (c) in the case of an asymmetric system.

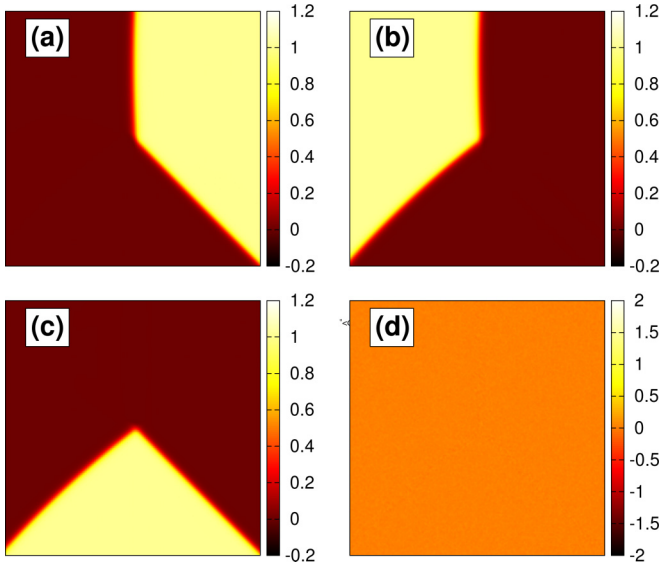

FIG. 5. Spatial distribution of the individual components (a)–(c) in the vicinity of the equilibrium trijunction in an asymmetric ternary system, and (d) error of the local sum of the variables, $e := 10^{14}[\sum_{i=1}^{3} c_i(\mathbf{r}) - 1]$. Note that the third component is not present at the binary interfaces, while the error of the local sum is negligible.

A. Contact angles

The validation of the model started with equilibrium contact angle measurements in both symmetric ($\hat{\sigma}_{ij} = \hat{\delta}_{ij} = 1$) and asymmetric systems. As discussed in Sec. III, the function $h(c_i,c_j) = |c_i/(1-c_i)||c_j/(1-c_j)|$ in Eq. (36) might generate "dangerous" solutions (i.e., stationary solutions that do not represent equilibrium), therefore the dynamic equations were solved by applying $h(c_i,c_j) \equiv 1$ (and $\hat{\kappa}_{ij} = 1/2$) in this case. Since we are interested exclusively in equilibrium, but not the time evolution of the system, this step does not influence the results. The initial condition for the velocity field was $\mathbf{v}(\mathbf{r},0) = 0$, while the initial distribution of the components is shown in Fig. 4(a). For better visualization, $h_3(\mathbf{r},t) := \sum_{i=1}^{3} c_i(\mathbf{r},t)[(i-0.5)/3]$ is shown, thus indicating bulk components at $h = 1/6$, $1/2$, and $5/6$ for $i = 1$, 2, and 3, respectively. The calculations were performed on a 1024×1024 grid with time step $\Delta t = 0.001$. After 10^6 time steps, the flow field vanished, and the system practically reached equilibrium [the convergence criterion for equilibrium was $\bar{v} := 1/(N_x N_y)\sum_{i,j}\sqrt{\mathbf{v}_{i,j}^2} < 10^{-4}$ for the average velocity, which corresponds to 1 pixel shift in the solution in 10^6 time steps]. The amplitude of the triplet term was $A_3 = 0$ and $1/2$ in the symmetric and asymmetric system, respectively.

To measure the contact angles at a trijunction, we plotted the $c_i(\mathbf{r}) = 1/2$ contours for $i = 1$, 2, and 3, as shown in Fig. 4(c), and then we fitted straight lines (dashed in the figure) for the unperturbed binary interfaces ("far" from the trijunction). The crossing point of these lines defines the trijunction point. As expected, the contact angle $\alpha_1 = \alpha_2 = \alpha_3 = 120^\circ$ was detected in the symmetric system. In contrast, asymmetric systems establish different contact angles. For instance, for the interface tensions $\hat{\sigma}_{12} = 1.2$, $\hat{\sigma}_{13} = 1.0$, and $\hat{\sigma}_{23} = 0.8$ (the corresponding interface thicknesses were $\hat{\delta}_{12} = 1.1$, $\hat{\delta}_{13} = 0.9$, and $\hat{\delta}_{23} = 1.0$, respectively), the theoretical contact angles can be determined from the condition of mechanical equilibrium, yielding

$$\alpha_1^0 = \pi - \cos^{-1}\left(\frac{\hat{\sigma}_{12}^2 + \hat{\sigma}_{13}^2 - \hat{\sigma}_{23}^2}{2\hat{\sigma}_{12}\hat{\sigma}_{13}}\right) = 138.6^\circ, \quad (55)$$

$$\alpha_2^0 = \pi - \cos^{-1}\left(\frac{\hat{\sigma}_{12}^2 + \hat{\sigma}_{23}^2 - \hat{\sigma}_{13}^2}{2\hat{\sigma}_{12}\hat{\sigma}_{23}}\right) = 124.23^\circ, \quad (56)$$

$$\alpha_3^0 = \pi - \cos^{-1}\left(\frac{\hat{\sigma}_{13}^2 + \hat{\sigma}_{23}^2 - \hat{\sigma}_{12}^2}{2\hat{\sigma}_{13}\hat{\sigma}_{23}}\right) = 97.181^\circ. \quad (57)$$

From the simulation, the contact angles $\alpha_1 = 137.3^\circ$, $\alpha_2 = 126.37^\circ$, and $\alpha_3 = 96.33^\circ$ have been measured [see Fig. 4(d)], showing then 1.7% maximal relative error compared to the theoretical values, which can be attributed to the uncertainty of the measurement.

Figure 5 shows the individual compositions [panels (a)–(c)] and the sum of the fields [panel (d)] in the neighborhood of the trijunction displayed in Fig. 4(d). The spatial distribution of the individual fields demonstrates the effect of the triplet term. In accordance with Figs. 3(b) and 4(d), all of the two-component interfaces are practically free of the third component. Furthermore, Fig. 5(d) shows that the error of the local sum of the variables is in the range of the truncation error of double-precision floating point numbers.

The calculations were repeated in an asymmetric four-component (quaternary) system as well (see Fig. 6), with $\hat{\sigma}_{12} = 1.0$, $\hat{\sigma}_{13} = 1.1$, $\hat{\sigma}_{14} = 0.75$, $\hat{\sigma}_{23} = 0.9$, $\hat{\sigma}_{24} = 1.25$, and $\hat{\sigma}_{34} = 1.0$. The interface thicknesses were equal, i.e., $\hat{\delta}_{ij} = 1.0$ was used, while the amplitude of the triplet term was $A_3 = 1$. The contact angle measurements resulted in less than 1.5%

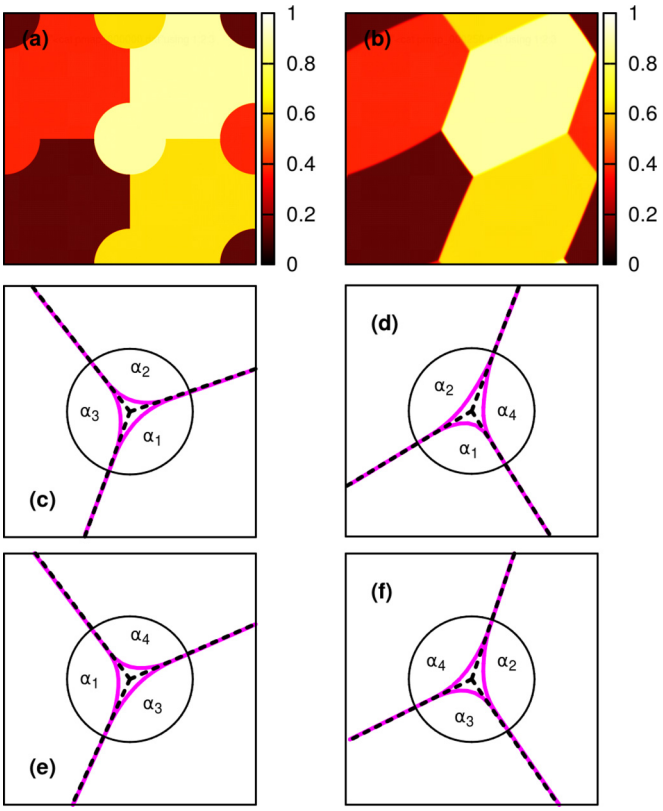

FIG. 6. Contact angles in an asymmetric quaternary system (for parameters, see the main text): (a) initial condition, (b) equilibrium state, and (c) and (d) contour lines for the fields in the vicinity of the four different trijunctions from panel (b), analogously to Fig. 4. In panels (a) and (b), $h_4(\mathbf{r},t) = \sum_{i=1}^{4}[(i-1/2)/4]c_i(\mathbf{r},t)$ is shown.

relative error again compared to the theoretical values for all four different trijunctions [illustrated in Figs. 6(c)–6(f)]. According to our experience, the unperturbed binary planar interfaces contain no additional components, similarly to the ternary case.

B. Spinodal decomposition

Since we are now interested in the time evolution of the system, the modified Bollada-Jimack-Mullis matrix defined by Eq. (15) is used henceforth.

1. Binary system

Spinodal decomposition was studied first in the binary limit. Technically, we performed calculations in a ternary system, where the third component was set to 0 initially, i.e., $c_3(\mathbf{r},0) = 0$ was used. In this case, the dynamic equations, together with the Navier-Stokes equation, naturally reduce to the dynamic equations of a traditional, one order parameter flow-assisted Cahn-Hilliard system. Therefore, the reference calculation was based on the surfactant-assisted liquid phase separation model of Tóth and Kvamme for incompressible liquid flow in the surfactant-free case. The dynamic equations read

$$\dot{\phi} = \nabla^2[(\phi^3 - \phi) - 2\nabla^2\phi], \tag{58}$$

$$\dot{\mathbf{v}} = \nabla\cdot(\mathbb{A} + \mathbb{D}), \tag{59}$$

$$\mathbb{A} = -2\,\tilde{w}\,(\nabla\phi\otimes\nabla\phi), \tag{60}$$

$$\mathbb{D} = \tilde{\mu}[(\nabla\otimes\mathbf{v}) + (\nabla\otimes\mathbf{v})^T], \tag{61}$$

$$0 = \nabla\cdot\mathbf{v}. \tag{62}$$

The transformation of the fields read $c_1 = (1+\phi)/2$ and $c_2 = (1-\phi)/2$, yielding $\hat{\kappa}_{12}^0 = 1$, $\hat{\eta} = \hat{\eta}_0(c_1\,x_1 + c_2\,x_2)$ corresponding to $\tilde{\mu} = \tilde{\mu}_0[x_1(1+\phi)/2 + x_2(1-\phi)/2]$ with $\hat{\eta}_0 = \tilde{\mu}_0$, and $\hat{a} = 4\tilde{w}$. We used $\tilde{\mu}_0 = 2857.0$, $x_1 = 1.0$, and $x_2 = 1633.0/\tilde{\mu}_0$ in Eq. (54), and $\tilde{w} = 1.73\times10^4$. The initial condition was $\phi(\mathbf{r},0) = A\,\mathcal{R}[-1,+1]$ [and $c_1(\mathbf{r},0) = 0.5 + (A/2)\mathcal{R}[-1,+1]$, correspondingly], where $\mathcal{R}[-1,1]$ is a uniformly distributed random number on $[-1,1]$, and $|A| \ll 1$. Since the homogeneous state $\phi = 0$ (and $c_1 = 0.5$) represents unstable equilibrium, the system undergoes phase separation for $A \neq 0$. Since the implementation of the equations in solving the different models is different, we do not expect exactly the *same* result from the same initial condition. Nevertheless, we are interested only in the characteristic behavior of the system. Therefore, we used different random numbers (but the same amplitude A) in setting up the initial conditions for ϕ and c_1. In this case, $\Delta t = 0.0025$ was chosen. Snapshots of the simulations are presented in Fig. 7. It is quite clear that the patterns roughen similarly as a function of time in both cases, indicating that the dynamic equations of the present model reduce naturally to the conventional binary model. In addition, no appearance of the third component was detected in our model during the simulation, due to the Bollada-Jimack-Mullis-type mobility matrix.

2. Asymmetric ternary and quaternary flows

In our first multicomponent simulation, an asymmetric ternary system was considered with dimensionless interfacial tensions $\hat{\sigma}_{12} = 1.2$, $\hat{\sigma}_{13} = 1.0$, and $\hat{\sigma}_{23} = 0.8$, and dimensionless interface thicknesses $\hat{\delta}_{12} = 1.1$, $\hat{\delta}_{13} = 0.9$, and $\hat{\delta}_{23} = 1.0$. The amplitude of the triplet term was $A_3 = 1/2$, which was enough to stabilize the binary planar interfaces. The pairwise diffusion constants were also asymmetric. We used $\hat{D}_{12} = 1.0$, $\hat{D}_{13} = 2.0$, and $\hat{D}_{23} = 0.5$, whereas the dimensionless viscosities in Eq. (54) were $x_1 = 0.5$, $x_2 = 1.0$, and $x_3 = 2.0$, respectively. The initial condition reads $c_1(\mathbf{r},0) = 0.2 + A\,\mathcal{R}[-1,1]$, $c_2(\mathbf{r},0) = 0.3 + A\,\mathcal{R}[-1,1]$, and $c_3(\mathbf{r},0) = 1 - [c_1(\mathbf{r},0) + c_2(\mathbf{r},0)]$, where $A = 0.01$ was chosen. The simulation has been performed on a 1024×1024 computational grid with $h = 0.5$ and $\Delta t = 0.005$. Snapshots of the simulation are shown in Figs. 8(a)–8(d) at different dimensionless times. As one can see, the system is unstable in its initial state, and it undergoes spinodal decomposition. Although the system is still far from equilibrium at $t = 3125$, the individual fields of the components [see panels (e)–(g)] suggest that the third component vanishes at the evolving binary interfaces. It is nevertheless important to mention that pure binary interfaces exist only in equilibrium,

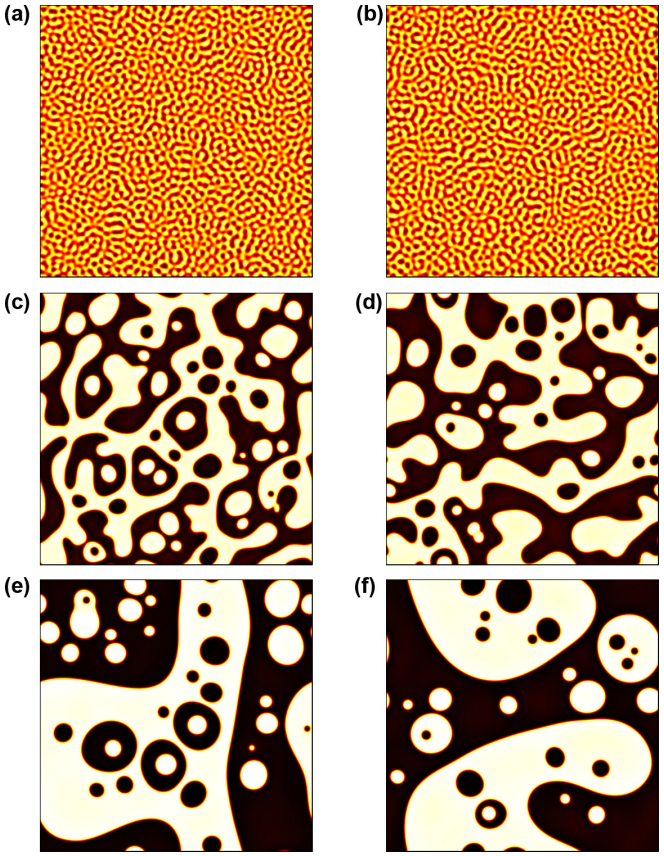

FIG. 7. Pattern coarsening during liquid-flow-assisted spinodal decomposition of a binary liquid, as predicted by the Ginzburg-Landau theory of surfactant-assisted liquid phase separation of Tóth and Kvamme (left column) and the present model (right column). The snapshots of the simulations were taken at $t = 62.5$, 125, and 250, respectively (from top to bottom).

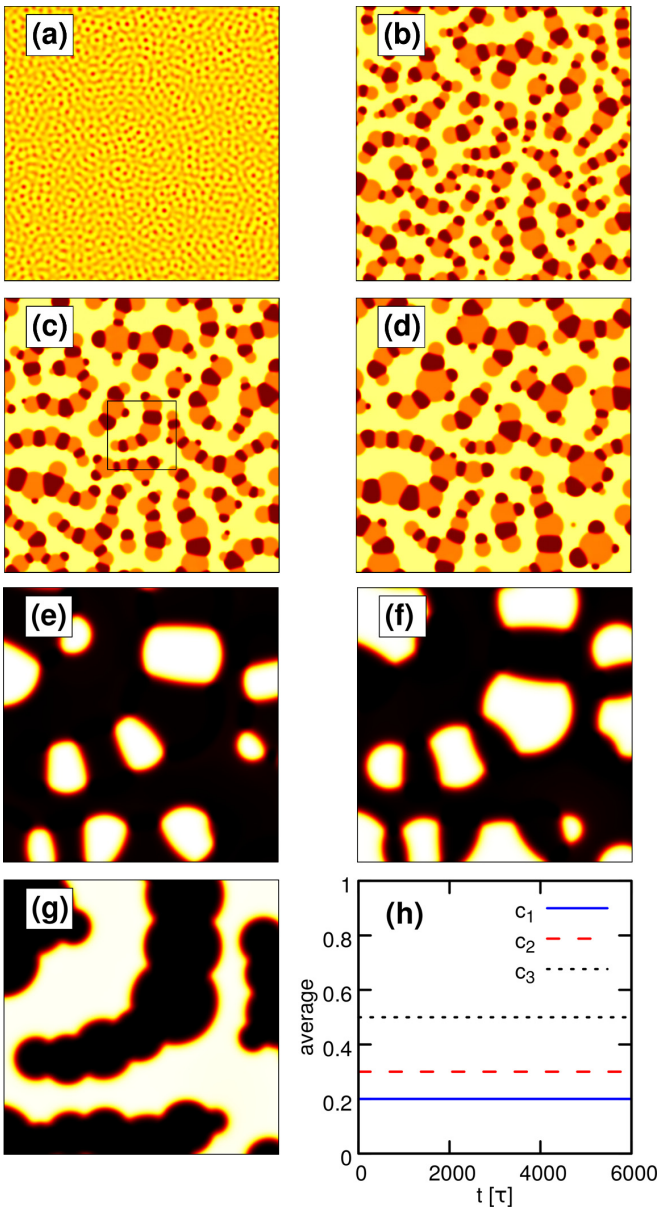

FIG. 8. Spinodal decomposition in an asymmetric ternary system. Snapshots of the simulation at $t = 312.5$, 1250, 3125, and 6250 [from panels (a) to (d)], respectively. Coloring is the same as in Fig. 6. Panels (e)–(g) show the individual mass fractions $c_1(\mathbf{r},t)$, $c_2(\mathbf{r},t)$, and $c_3(\mathbf{r},t)$, respectively, in the area indicated by the black square in panel (c). (Black corresponds to $c = 0$ and white to $c = 1$.) The time evolution of the total concentrations is shown in panel (h), thus indicating global conservation for all components.

while nonequilibrium curved interfaces may contain the third component. This effect is not prevented by applying a mobility matrix of the Bollada-Jimack-Mullis type, which is responsible only for preventing the appearance of a component when it is not present in a calculation *at all* [26]. Nevertheless, the third component tends to vanish at even nonequilibrium curved interfaces, showing the robustness of the construction of the free-energy functional.

The simulations were repeated in a quaternary system as well (see Fig. 9), where the dimensionless interfacial tensions were $\hat{\sigma}_{12} = 1.0$, $\hat{\sigma}_{13} = 1.1$, $\hat{\sigma}_{14} = 0.75$, $\hat{\sigma}_{23} = 0.9$, $\hat{\sigma}_{24} = 1.25$, and $\hat{\sigma}_{34} = 1.0$, while all interface thicknesses and diffusion constants were chosen to be equal, i.e., $\hat{\delta}_{ij} = \hat{D}_{ij} = 1.0$. Furthermore, we chose $A_3 = 1.0$ to stabilize all the binary planar interfaces. The dimensionless viscosities were $x_1 = x_3 = 1.0$, $x_2 = 0.5$, and $x_4 = 2.0$, respectively. Our experience was quite the same as in the ternary case: The system prepared in a high-energy, strongly nonequilibrium, homogeneous multicomponent state undergoes phase separation, which is enhanced by the liquid flow. In the forming pattern, the bulk—interface—trijunction topology dominates, as expected from the free-energy functional and the energy minimizing dynamics. Furthermore, the additional components vanish at evolving interfaces and trijunctions in time. The forming patterns are also quite similar in the two cases, mostly doe to the fact that we had a majority component (c_3 and c_4 in the ternary and quaternary system, respectively) in which "bubbles" of the minority phases started to form. The final (equilibrium) pattern, however, remains a question: the system has to find a configuration containing the lowest possible amount of interfaces and trijunctions, and representing the minimum of the free-energy functional. Such a configuration, nevertheless, can be a strong function of the volume fractions of the components. For example, in a binary system with a

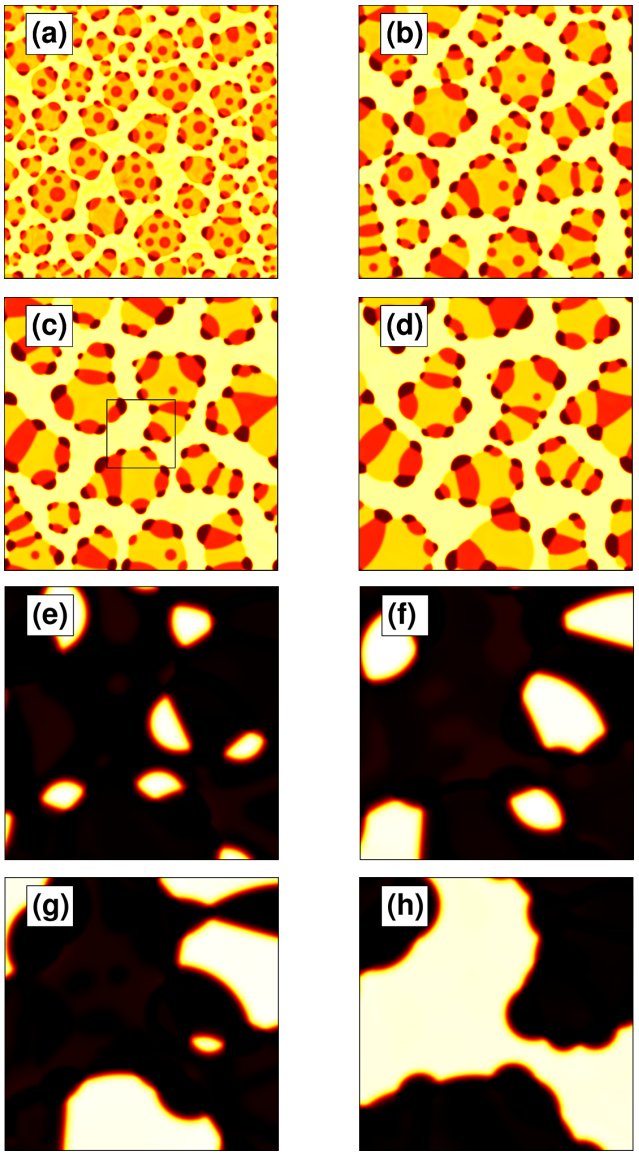

FIG. 9. Spinodal decomposition in an asymmetric quaternary (four-component) system. Snapshots at dimensionless times $t =$ 312.5, 1250, 3125, and 6250, respectively. The individual fields $c_1(\mathbf{r},t)$, $c_2(\mathbf{r},t)$, $c_3(\mathbf{r},t)$, and $c_4(\mathbf{r},t)$ are shown in panels (e) and (f) in the black square indicated in panel (c).

volume fraction $1/2 : 1/2$, two binary planar interfaces should form, while in a system of volume fraction $1/10 : 9/10$, for example, it is not energetically preferred to create such long interfaces. Instead, a bubble of the minority component forms, thus representing lower energy. In multicomponent systems, the solution of the Euler-Lagrange equations can even be degenerate, i.e., it might have multiple solutions representing local minima in which the system can be trapped.

Comparing Figs. 8 and 9 sheds light on an another important detail. At $t = 312.5$ [panel (a) in both figures], the ternary system is still almost homogeneous, at least compared to the quaternary system, which shows a much more developed pattern. Although both systems had similar initial conditions, $A = 1/2$ and 1 were used in the ternary and quaternary case, respectively. This, together with Figs. 1(c) and 1(d), give a good impression of how the triplet term works: increasing A_3 means increasing penalization for multicomponent states (ternary *and* above, as discussed in Sec. III B), which forces the system to get rid of the multicomponent states faster and faster. Indeed, $A_3 = 1$ (Fig. 9) means a stronger penalization than $A_3 = 1/2$ (Fig. 8), therefore the quaternary system eliminates the high-order states.

The long-time effect of A_3 on the evolving pattern is, however, expected to be negligible. As long as A_3 is roughly in the same order of magnitude as $\max[g(\mathbf{c})]$, small perturbations around binary interfaces produce small variation in the energy relative to the interfacial tension. The key is, again, that the triplet term is used solely to stabilize the binary planar interfaces, thus resulting in a strongly finite A_3. In contrast, in previous multiphase/multicomponent descriptions, the binary interfaces are not equilibrium solutions, and the triplet term is applied to suppress the third component, which is definitely present at the binary planar interface. In these cases, the binary planar interface solution is recovered for $A_3 \to \infty$, which then may significantly affect the dynamics of the quasibinary interfaces even if only a small amount of the third component is present. Summarizing, the purpose of applying the triplet term is essentially different in the two cases.

VI. CONCLUSIONS

In this work, we presented a generalization of the Cahn-Hilliard theory of liquid phase separation for an arbitrary number of components. It has been shown that the generalization can be done in a systematic way. First, a general physically and mathematically consistent entropy producing advection-diffusion dynamics has been set up, which then has been extended with the generalization of the Cahn-Hilliard free-energy functional for many components. The extension has been done on a phenomenological basis, resulting in a model, that (i) reduces/extends naturally on the level of both the free-energy functional and the dynamic equations when removing/adding a component, and (ii) recovers the standard Cahn-Hilliard model for $N = 2$. Furthermore, (iii) the bulk states and the two-component interfaces are *stable* equilibrium solutions of the multicomponent model, (iv) the free-energy functional penalizes the high-order multicomponent states strictly monotonously as a function of the number of components being present, and (v) the pairwise interfacial properties (interfacial tension and interface thickness) can be chosen independently.

We have shown that (i) a simple triplet energy term can be used to *stabilize the binary planar interfaces*, and (ii) the equilibrium contact angles are in perfect agreement with theoretical values. Furthermore, we demonstrated that (iii) the system undergoes spinodal decomposition when starting from a high-energy nonequilibrium state, and it converges to equilibrium by developing the bulk—interface—trijunction topology in two dimensions in asymmetric ternary and quaternary systems.

Our results might contribute significantly to the continuum theory of multicomponent liquids, since controlled pattern formation in these systems is of increasing importance in several practical applications. For instance, surfactant controlled nanoshell formation opened a new chapter in

targeted drug delivery [33]. Another crucial field is energy, namely a controlled emulsion→emulsion transition in the CO_2-water-heavy crude oil system, would result in an efficient and environmentally sound combination of CO_2 storage and enhanced oil recovery [34,35].

ACKNOWLEDGMENTS

The authors thank László Gránásy and Tamás Pusztai from the Wigner Research Center for Physics, Hungary, Valeriy I. Levitas from Iowa State University, and Kumar Ankit from Karlsruhe University, Germany. This work has been supported by the VISTA basic research programme Project No. 6359 "Surfactants for water-CO_2-hydrocarbon emulsions for combined CO_2 storage and utilization" of the Norwegian Academy of Science and Letters and the Statoil.

APPENDIX A: ENERGY HIERARCHY

In a symmetric system, the free-energy landscape reads

$$\frac{f(\mathbf{c})}{w_0} = g(\mathbf{c}) + a\, f_3(\mathbf{c}), \tag{A1}$$

where

$$g(\mathbf{c}) = \frac{1}{12} + \sum_{i=1}^{N}\left(\frac{c_i^4}{4} - \frac{c_i^3}{3}\right) + \frac{1}{2}\sum_{i<j}(c_i c_j)^2, \tag{A2}$$

$a = A_3/w_0 \geqslant 0$, and

$$f_3(\mathbf{c}) = \sum_{i<j<k}^{N,N,N} |c_i|\,|c_j|\,|c_k|. \tag{A3}$$

For $\mathbf{c}_n = \mathbb{P}[(1/n,1/n,\ldots,1/n,0,0,\ldots,0)]$, Eq. (A1) reads

$$f(n) = \frac{1}{12}\left(1 - \frac{1}{n^2}\right) + a\left[\frac{n(n-1)(n-2)}{6}\left(\frac{1}{n}\right)^3\right], \tag{A4}$$

which must be monotonously increasing as a function of $n = 1,2,3,\ldots$. The increment for $n \to n+1$ components then reads

$$f(n+1) - f(n) = \frac{1 + 2n + 2a\,(n-1)(2+3n)}{12\,n^2(1+n)^2} \geqslant 0, \tag{A5}$$

which is trivially true for $n \geqslant 1$ and $a \geqslant 0$. We note, however, that this tendency is not true for higher-order triplet terms, such as $(c_i c_j c_k)^2$, for example, when $f(n)$ shows a maximum for any positive A_3.

APPENDIX B: EQUILIBRIUM SOLUTIONS

In the multicomponent system, thermodynamic equilibrium is defined by the extrema of the free-energy functional. The corresponding Euler-Lagrange equations of the complete multicomponent problem read

$$\nabla\frac{\delta F}{\delta c_i} = \nabla\frac{\delta F}{\delta c_j} \tag{B1}$$

for any $i \neq j$ pairs, $i,j = 1,\ldots,N$. The functional derivatives read

$$\frac{\delta F}{\delta c_i} = \frac{\partial f}{\partial c_i} - \nabla\frac{\partial f}{\partial \nabla c_i}, \tag{B2}$$

where

$$f = w(\mathbf{c})\, g(\mathbf{c}) + A_3\, f_3(\mathbf{c}) + \frac{\epsilon^2(\mathbf{c})}{2}\sum_{i=1}^{N}(\nabla c_i)^2 \tag{B3}$$

is the integrand of the free-energy functional defined by Eq. (23). Using this in Eq. (B2) yields

$$\frac{\delta F}{\delta c_i} = \frac{\partial w}{\partial c_i}g(\mathbf{c}) + \frac{\partial \epsilon^2}{\partial c_i}\left[\frac{1}{2}\sum_{i=1}^{N}(\nabla c_i)^2\right] + w(\mathbf{c})\frac{\partial g}{\partial c_i} + A_3\frac{\partial f_3}{\partial c_i} - \nabla\cdot[\epsilon^2(\mathbf{c})\nabla c_i], \tag{B4}$$

where

$$\frac{\partial \epsilon^2}{\partial c_i} = 2\,c_i\frac{\sum_{j\neq i}\left[\epsilon_{ij}^2 - \epsilon^2(\mathbf{c})\right]c_j^2}{\sum_{k<l} c_k^2 c_l^2}, \tag{B5}$$

$$\frac{\partial w}{\partial c_i} = 2\,c_i\frac{\sum_{j\neq i}[w_{ij} - w(\mathbf{c})]c_j^2}{\sum_{k<l} c_k^2 c_l^2}, \tag{B6}$$

$$\frac{\partial g}{\partial c_i} = c_i(\mathbf{c}^2 - c_i), \tag{B7}$$

$$\frac{\partial f_3}{\partial c_i} = \mathrm{sgn}(c_i)\sum_{(j<k)\neq i}|c_j|\,|c_k|. \tag{B8}$$

Since Eq. (B4) vanish for $c_i(\mathbf{r}) = 0$, the functional derivative vanishes for a vanishing field, i.e., $(\delta F/\delta c_i)_{c_i=0} = 0$. Therefore, in the binary limit $c_I(\mathbf{r}) + c_J(\mathbf{r}) = 1$ and $c_K(\mathbf{r}) = 0$, the functional derivatives read

$$\frac{\delta F}{\delta c_I} = w_{IJ}\frac{\partial g}{\partial c_I} - \epsilon_{IJ}^2\nabla^2 c_I, \tag{B9}$$

$$\frac{\delta F}{\delta c_J} = w_{IJ}\frac{\partial g}{\partial c_J} - \epsilon_{IJ}^2\nabla^2 c_J, \tag{B10}$$

$$\frac{\delta F}{\delta c_K} = 0, \tag{B11}$$

where $\partial g/\partial c_I = -\partial g/\partial c_J = c_I\{[c_I^2 + (1-c_I)^2] - c_I\} = c_I(1-c_I)(1-2c_I)$, i.e., $\frac{\partial g}{\partial c_I}|_{c_I+c_J=1} = \{\frac{\partial}{\partial c}[c^2(1-c)^2]\}_{c=c_I}$. It is easy to see that the triplet term has no contribution to the free energy at all, since only two components are present, while $\mathrm{sgn}(0) = 0$ ensures the vanishing derivative in the equation for vanishing c_K. In addition, the derivatives of the Kazaryan polynomials also vanish for $c_I + c_J = 1$, since in this case the sums in the nominators vanish. Substituting $c_I(x) = \{1 + \tanh[x/(2\,\delta_{IJ})]\}/2$, $c_J(x) = 1 - c_I(x)$, and $c_K(x) = 0$ into Eqs. (B9) and (B10) then yields

$$\delta F/\delta c_i = 0 \tag{B12}$$

for $i = 1,\ldots,N$, i.e., the binary planar interfaces are equilibrium solutions of the multicomponent problem.

[1] M. F. Haase and J. Brujic, Tailoring of high-order multiple emulsions by the liquid-liquid phase separation of ternary mixtures, Angew. Chem. **126**, 11987 (2014).

[2] T. Shukutani, T. Myojo, H. Nakanishi, T. Norisuye, and Q. Tran-Cong-Miyata, Tricontinuous morphology of ternary polymer blends driven by photopolymerization: Reaction and phase separation kinetics, Macromolecules **47**, 4380 (2014).

[3] G. Ahearn, Surfactants for oil recovery, J. Am. Oil Chem. Soc. **46**, 540A (1969).

[4] S. Iglauer, Y. Wu, P. Shuler, Y. Tang, and W. A. G. III, New surfactant classes for enhanced oil recovery and their tertiary oil recovery potential, J. Pet. Sci. Eng. **71**, 23 (2010).

[5] S. Q. Tunio, A. H. Tunio, N. A. Ghirano, and Z. M. El Adawy, Comparison of different enhanced oil recovery techniques for better oil productivity, Int. J. Appl. Sci. Technol. **1**, 143 (2011).

[6] Z. Song, Z. Li, M. Wei, F. Lai, and B. Bai, Sensitivity analysis of water-alternating-co^2 flooding for enhanced oil recovery in high water cut oil reservoirs, Comput. Fluids **99**, 93 (2014).

[7] J. W. Cahn and J. E. Hilliard, Free energy of a nonuniform system. i. interfacial free energy, J. Chem. Phys. **28**, 258 (1958).

[8] H. Cook, Brownian motion in spinodal decomposition, Acta Metall. **18**, 297 (1970).

[9] J. Langer, Theory of spinodal decomposition in alloys, Ann. Phys. **65**, 53 (1971).

[10] J. Langer, Statistical methods in the theory of spinodal decomposition, Acta Metall. **21**, 1649 (1973).

[11] D. D. Fontaine, An analysis of clustering and ordering in multicomponent solid solutions—i. Stability criteria, J. Phys. Chem. Solids **33**, 297 (1972).

[12] D. D. Fontaine, An analysis of clustering and ordering in multicomponent solid solutions—ii. Fluctuations and kinetics, J. Phys. Chem. Solids **34**, 1285 (1973).

[13] J. Morral and J. Cahn, Spinodal decomposition in ternary systems, Acta Metall. **19**, 1037 (1971).

[14] J. Hoyt, Spinodal decomposition in ternary alloys, Acta Metall. **37**, 2489 (1989).

[15] J. Hoyt, Linear spinodal decomposition in a regular ternary alloy, Acta Metall. Mater. **38**, 227 (1990).

[16] S. Maier-Paape, B. Stoth, and T. Wanner, Spinodal decomposition for multicomponent Cahn-Hilliard systems, J. Stat. Phys. **98**, 871 (2000).

[17] D. J. Korteweg, Sur la forme que prennent les équations du mouvement des uides si l'ontient compte des forces capillaires causées par des variations de densité considérables mais continues et sur la théorie de la capillarité dans l'hypothése d'une variation continue de la densité, Arch. Neerl. Sci. Ex. Nat. **6**, 1 (1901).

[18] R. Evans, The nature of the liquid-vapour interface and other topics in the statistical mechanics of non-uniform, classical fluids, Adv. Phys. **28**, 143 (1979).

[19] R. Salmon, Hamiltonian fluid mechanics, Annu. Rev. Fluid Mech. **20**, 225 (1988).

[20] A. A. Wheeler and G. B. McFadden, On the notion of a ξ-vector and a stress tensor for a general class of anisotropic diffuse interface models, Proc. R. Soc. London, Ser. A **453**, 1611 (1997).

[21] D. Anderson, G. McFadden, and A. Wheeler, A phase-field model of solidification with convection, Physica D **135**, 175 (2000).

[22] D. M. Anderson, G. B. McFadden, and A. A. Wheeler, Diffuse-interface methods in fluid mechanics, Annu. Rev. Fluid Mech. **30**, 139 (1998).

[23] G. Tegze, T. Pusztai, and L. Gránásy, Phase field simulation of liquid phase separation with fluid flow, Mater. Sci. Eng. A **413-414**, 418 (2005), International Conference on Advances in Solidification Processes.

[24] J. Kim and J. Lowengrub, Phase field modeling and simulation of three-phase flows, Int. Free Bound. **7**, 435 (2005).

[25] J. Kim, Phase-field models for multi-component fluid flows, Commun. Comput. Phys. **12**, 613 (2012).

[26] G. I. Tóth, T. Pusztai, and L. Gránásy, Consistent multiphase-field theory for interface driven multidomain dynamics, Phys. Rev. B **92**, 184105 (2015).

[27] L. Onsager, Theories and problems of liquid diffusion, Ann. N.Y. Acad. Sci **46**, 241 (1945).

[28] P. Bollada, P. Jimack, and A. Mullis, A new approach to multi-phase formulation for the solidification of alloys, Physica D **241**, 816 (2012).

[29] A. Kazaryan, Y. Wang, S. A. Dregia, and B. R. Patton, Generalized phase-field model for computer simulation of grain growth in anisotropic systems, Phys. Rev. B **61**, 14275 (2000).

[30] K. Ankit, B. Nestler, M. Selzer, and M. Reichardt, Phase-field study of grain boundary tracking behavior in crack-seal microstructures, Contrib. Mineral. Petrol. **166**, 1709 (2013).

[31] V. I. Levitas and A. M. Roy, Multiphase phase field theory for temperature- and stress-induced phase transformations, Phys. Rev. B **91**, 174109 (2015).

[32] G. Tegze, G. Bansel, G. I. Tóth, T. Pusztai, Z. Fan, and L. Gránásy, Advanced operator splitting-based semi-implicit spectral method to solve the binary phase-field crystal equations with variable coefficients, J. Comput. Phys. **228**, 1612 (2009).

[33] M. M. De Villiers and Y. M. Lvov, Nanoshells for Drug Delivery, in *Nanotechnologies for the Life Sciences* (Wiley-VCH, Weinheim, Germany, 2007).

[34] G. I. Tóth and B. Kvamme, Analysis of Ginzburg-Landau-type models of surfactant-assisted liquid phase separation, Phys. Rev. E **91**, 032404 (2015).

[35] G. I. Tóth and B. Kvamme, Phase field modeling of spinodal decomposition in the oil/water/asphaltene system, Phys. Chem. Chem. Phys. **17**, 20259 (2015).